20-Gb/s Modulation of Silicon-Integrated Short-Wavelength Hybrid-Cavity VCSELs

Emanuel P. Haglund, *Student Member, IEEE*, Sulakshna Kumari, Petter Westbergh, Johan S. Gustavsson, Roel G. Baets, *Fellow, IEEE*, Gunther Roelkens, *Member, IEEE*, and Anders Larsson, *Fellow, IEEE*

***Abstract*— We investigate the dynamics of silicon-integrated 850-nm-wavelength hybrid-cavity vertical-cavity surface-emitting lasers (VCSELs). The VCSELs consist of a GaAs-based half-VCSEL attached to a dielectric distributed Bragg reflector on a silicon substrate using ultra-thin divinylsiloxane-bis-benzocyclobutene adhesive bonding. A 5-μm oxide aperture diameter VCSEL, with a small signal modulation bandwidth of 11 GHz, supports data transmission at bit rates up to 20 Gb/s. The modulation bandwidth and the large signal modulation characteristics are found to be impaired by the high thermal impedance.**

***Index Terms*— High-speed modulation, large signal modulation, optical interconnects, semiconductor lasers, silicon photonics, vertical-cavity surface-emitting laser (VCSEL).**

I. Introduction

SILICON photonics has emerged as a promising technology for future optical interconnects. Silicon's lack of efficient light emission calls for hybrid solutions. The most efficient high-speed light source available is the GaAs-based vertical-cavity surface-emitting laser (VCSEL), with modulation bandwidth up to 30 GHz [1], data rates above 70 Gb/s [2], and energy dissipation of less than 100 fJ/bit at data rates up to 50 Gb/s [1], [3].

While flip-chip bonding of VCSELs on silicon photonic chips has been explored [4], a more practical technique for integration of VCSELs on silicon is heterogeneous integration. This has previously been successfully demonstrated using InP-based structures attached to a silicon high-contrast grating on a silicon substrate [5], [6]. To date, small signal modulation bandwidths up to 2.5 GHz and large signal data transmission at bit rates up to 5 Gb/s have been demonstrated with heterogeneously integrated VCSELs [6].

Manuscript received September 9, 2015; revised December 1, 2015; accepted December 29, 2015. Date of publication January 6, 2016; date of current version March 10, 2016. This work was supported in part by the Swedish Foundation for Strategic Research and in part by the FP7-ERC-InSpectra Advanced Grant.

E. P. Haglund, P. Westbergh, J. S. Gustavsson, and A. Larsson are with the Photonics Laboratory, Department of Microtechnology and Nanoscience, Chalmers University of Technology, Gothenburg SE-412 96, Sweden (e-mail: emanuel.haglund@chalmers.se; petter.westbergh@chalmers.se; johan.gustavsson@chalmers.se; anders.larsson@chalmers.se).

S. Kumari, R. G. Baets, and G. Roelkens are with the Photonics Research Group, Center for Nano- and Biophotonics, Ghent B-9000, Belgium (e-mail: sulakshna.kumari@intec.ugent.be; roel.baets@intec.ugent.be; gunther.roelkens@intec.ugent.be).

Color versions of one or more of the figures in this letter are available online at http://ieeexplore.ieee.org.

Digital Object Identifier 10.1109/LPT.2016.2514699

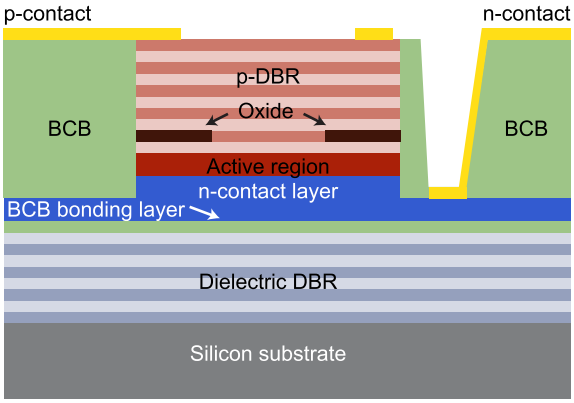

Fig. 1. Schematic cross-section of the hybrid-cavity VCSEL design.

Recently, we demonstrated a silicon-integrated short-wavelength hybrid-cavity VCSEL, as a potential light source for silicon nitride (SiN) waveguide circuits, where a GaAs-based "half-VCSEL" is attached to a dielectric distributed Bragg reflector (DBR) on a silicon substrate (Fig. 1 and [7]). This configuration results in a surface emitting laser. Coupling to an in-plane SiN waveguide on top of the dielectric DBR can be accomplished by a weak intra-cavity diffraction grating etched in the waveguide layer [8]. It can also be accomplished by using a high-contrast SiN grating reflector (instead of the dielectric DBR) connected to the in-plane SiN waveguide [9].

Here, we extend the analysis of the hybrid-cavity VCSEL to an investigation of its dynamic characteristics. In particular, it allows us to investigate the impact of high thermal impedance, commonly associated with the integration schemes described above, on the VCSEL dynamics. While the high thermal impedance is found to have an impact on the dynamics, a VCSEL with 5 μm oxide aperture diameter, having a small signal modulation bandwidth exceeding 11 GHz, is used to transfer data at bit rates up to 20 Gb/s.

The letter is organized as follows. Section II covers the VCSEL design and the static characteristics, whereas the small signal modulation response and an analysis of speed limitations are presented in Section III. Large signal data transmission experiments are presented in Section IV and the letter is concluded in Section V.

II. VCSEL Design and Static Characteristics

The 850-nm-wavelength hybrid-cavity VCSEL design is illustrated in Fig. 1. The "half-VCSEL" epitaxial structure was

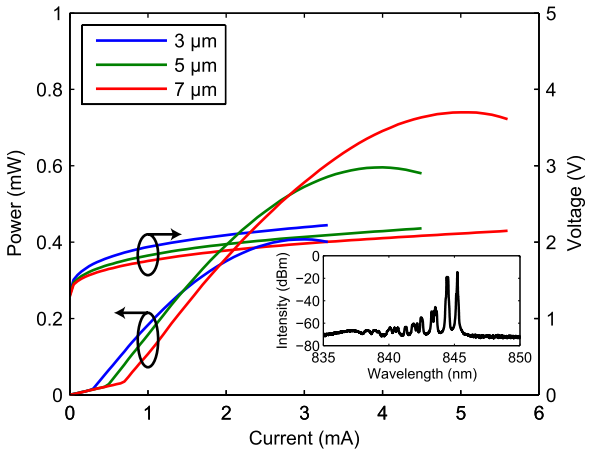

Fig. 2. Light-current-voltage characteristics measured at 25°C for hybrid-cavity VCSELs with oxide aperture diameters of 3, 5, and 7 μm. Inset: Emission spectrum for the 5 μm VCSEL biased at 3.5 mA.

grown on a GaAs substrate (at IQE Europe Ltd.) in the following order: a 23 pair p-doped $Al_{0.90}Ga_{0.10}As/Al_{0.12}Ga_{0.88}As$ DBR with an embedded 30 nm thick $Al_{0.98}Ga_{0.02}As$ layer to enable the formation of an oxide aperture, an active region with five 4 nm thick $In_{0.10}Ga_{0.90}As$ quantum wells (QWs), and an n-doped $Al_{0.12}Ga_{0.88}As$ intra-cavity contact and current spreading layer. The "half-VCSEL" epitaxial structure (8×10 mm die) was bonded to the 20 pair SiO_2/Ta_2O_5 dielectric DBR (with a total thickness of 4.9 μm and a theoretical reflectivity $>99.99\%$) on a 675 μm thick silicon wafer using ultra-thin (40 nm) divinylsiloxane-bis-benzocyclobutene (DVS-BCB) adhesive bonding [10], followed by removal of the GaAs substrate. VCSEL devices were then fabricated using a standard process for GaAs-based oxide-confined VCSELs. A thick layer of spin-coated BCB was used under the bondpads for low pad capacitance. A detailed description of the design and fabrication is presented in [7].

All measurements were performed with the VCSELs on a temperature-controlled heat-sink held at 25°C. The light-current-voltage characteristics of hybrid-cavity VCSELs with oxide aperture diameters of 3, 5, and 7 μm are shown in Fig. 2. The emission spectrum for the 5 μm aperture VCSEL, biased at 3.5 mA, is included as an inset to Fig. 2, showing lasing with multiple transverse modes around 845 nm. The threshold current is as low as 0.22 mA for the 3 μm oxide aperture VCSEL and the slope efficiency is $\sim$0.25 W/A for all aperture sizes, providing a maximum optical output power of 0.74 mW for the 7 μm oxide aperture VCSEL. Table I summarizes the static characteristics. The VCSELs presented in [7] have a thickness of the topmost layer in the p-DBR larger than $\lambda/4$. This results in a slightly out-of-phase reflection at the semiconductor-air interface which boosts the slope efficiency and the output power (reduced photon lifetime [11]). The VCSELs used here have a standard $\lambda/4$ thick top layer. Therefore, the threshold currents, slope efficiencies, and the maximum output powers are somewhat lower. The longer photon lifetime was found to be essential for achieving sufficient damping of the modulation response under large signal modulation and data transmission [12].

TABLE I
STATIC PERFORMANCE PARAMETERS

Oxide aperture diameter (μm)	Threshold current (mA)	Maximum optical output power (mW)	Thermal rollover current (mA)	Slope efficiency (W/A)	Differential resistance at thermal rollover (Ω)
3	0.22	0.41	3.4	0.23	88
5	0.38	0.60	4.0	0.25	73
7	0.57	0.74	5.0	0.25	59

As can be seen in Fig. 2, the VCSEL output power suffers from an early onset of the thermal rollover. With the dielectric materials having poor thermal conductivity (about two orders of magnitude lower than silicon), we attribute this to the limited heat transport through the dielectric DBR. The thermal impedance of the 5 μm oxide aperture VCSEL is 10.7 K/mW, measured by tracking the redshift of the fundamental optical mode with dissipated power and stage temperature. The thermal impedance is thus $\sim$3 times higher than for ordinary GaAs-based oxide-confined VCSELs [13]. Another contributor to the early thermal roll-over is the wavelength of the gain peak relative to the cavity resonance wavelength. The QW gain peak, estimated from the QW photoluminescence wavelength, is at $\sim$850 nm while the cavity resonance wavelength is at 843 nm. This results in minimum threshold current at an estimated temperature of -16°C [7].

III. SMALL SIGNAL MODULATION RESPONSE

The small signal modulation response (S_{21}) was measured with a 20 GHz vector network analyzer (Agilent N5230A) connected to the VCSEL under test through a high-speed bias-T and a high-speed RF probe (Picoprobe 40A-GSG-100P). The VCSEL was butt-coupled to an OM4 multimode optical fiber connected to a 28 GHz photodetector (Picometrix DG-32xr-FC). The measured data were corrected for the frequency response of the probe and photodetector.

Measured small signal modulation responses for the 3, 5, and 7 μm oxide aperture VCSELs are shown in Fig. 3 at four different bias currents. We attribute the low frequency roll-off of the modulation response, which is particularly pronounced at low bias currents, to overdamping from spatial hole burning [14]. This assumption is supported by the fact that the smaller aperture VCSELs with less number of transverse modes, which are more strongly affected by spatial hole burning, have a more pronounced roll-off. The maximum 3dB bandwidth, achieved at the highest bias currents indicated, is 11.7, 11.4, and 10.4 GHz for VCSELs with 3, 5, and 7 μm oxide aperture diameter, respectively.

By fitting a three-pole transfer function (which do not account for spatial hole burning) to the measured modulation response, the resonance frequency and the damping rate can be extracted [15]. These can then be used to calculate the K- and D-factors, as shown in Fig. 4. The K-factors are 0.2 ns for all three oxide aperture sizes, whereas the D-factors scale with the inverse of the aperture diameter and are 12.7, 7.2,

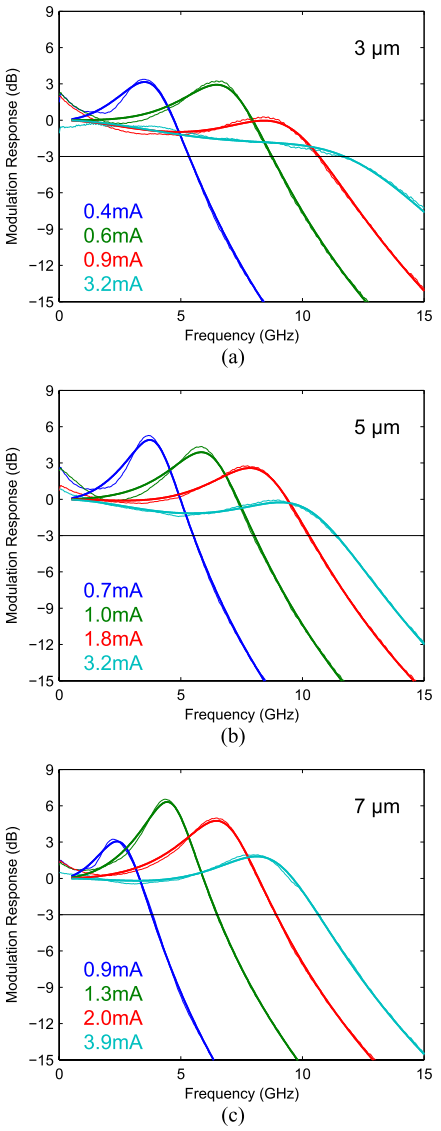

Fig. 3. Small signal modulation response of hybrid-cavity VCSELs with (a) 3, (b) 5, and (c) 7 μm oxide aperture diameter at indicated bias currents.

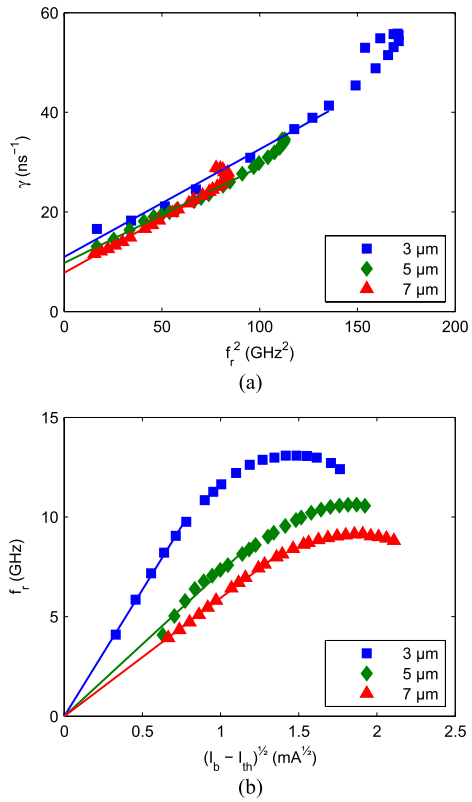

Fig. 4. (a) Damping rate versus resonance frequency squared, with linear fits to extract the K-factors (from the slope). (b) Resonance frequency versus square root of bias current above threshold, with linear fits to extract the D-factors (from the slope).

and 5.9 GHz/mA$^{1/2}$ for VCSELs with 3, 5, and 7 μm oxide aperture diameter, respectively. From the fit of the transfer function, a 5-6 GHz parasitic pole was also extracted. The low parasitic cut-off frequency is attributed to the high capacitance across the single oxide layer used in this VCSEL design and could thus be reduced by including additional oxide layers [16]–[18].

The intrinsic damping limited modulation bandwidth ($f_{3\text{dB,damping}}$), in the absence of parasitics and thermal effects, estimated from [15]

$$f_{3\text{dB,damping}} = 2\pi\sqrt{2}/K \tag{1}$$

exceeds 40 GHz. On the other hand, the thermally limited bandwidth ($f_{3\text{dB,thermal}}$), estimated from [15]

$$f_{3\text{dB,thermal}} = \sqrt{1+\sqrt{2}}\cdot f_{\text{r,max}} \tag{2}$$

where $f_{\text{r,max}}$ is the maximum resonance frequency, is only 16 GHz for the 5 μm aperture VCSEL. This is due to the early onset of the thermal rollover which prevents a sufficiently high photon density from being established in the cavity. With the resonance frequency (f_{r}) increasing with the photon density (S) according to [15]

$$f_{\text{r}} = \frac{1}{2\pi}\sqrt{\frac{v_{\text{g}}\cdot(\partial g/\partial n)\cdot S}{\tau_{\text{p}}}} \tag{3}$$

where v_{g} is the group velocity, $\partial g/\partial n$ is the differential gain, and τ_{p} is the photon lifetime, this limits the maximum resonance frequency. Therefore, in addition to parasitics, thermal effects impose a severe limitation on the modulation bandwidth.

For a conventional GaAs-based oxide-confined VCSEL, a K-factor of 0.2 ns would provide enough damping for a flat modulation response at high currents [12]. However, the present VCSELs exhibit significant peaking in the response also at high currents, as seen in Fig. 3. This again stems from the limited maximum photon density and resonance frequency (by the early onset of the thermal rollover), as the damping rate (γ) increases with resonance frequency according to [15]

$$\gamma = K\cdot f_{\text{r}}^2 + \gamma_0 \tag{4}$$

where (γ_0) is the damping offset. This imposes a limitation on the achievable bit rate under large signal modulation as the resonant response causes overshoot and ringing, which in turn translates into timing jitter and horizontal eye closure [12]. The smallest aperture VCSEL has a more damped

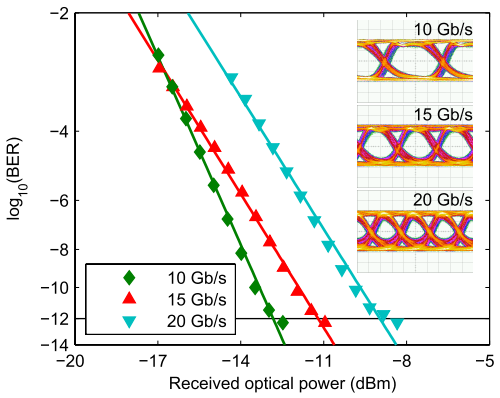

Fig. 5. BER measurements at 10, 15, and 20 Gb/s for a hybrid-cavity VCSEL with 5 μm oxide aperture diameter biased at 3.5 mA. Insets: Corresponding eye diagrams. Scales: 100 mV/div and 20 ps/div.

response (Fig. 3a), but its low output power limits the optical modulation amplitude, resulting in vertical eye closure at high bit rates.

IV. Data Transmission

The 5 μm oxide aperture VCSEL was used for large signal modulation and data transmission since it provides sufficiently high optical output power and has a moderately damped small signal modulation response. A non-return-to-zero signal consisting of pseudorandom binary sequences (PRBS) with word length 2^7-1, generated by a bit pattern generator (SHF 12103A), was fed to the VCSEL through the high-speed bias-T and the high-speed RF probe. The output light was coupled to an OM4 multimode optical fiber using a lens package. The fiber was connected to a 30 GHz limiting photoreceiver with an optical modulation amplitude sensitivity of -13dBm (VI Systems R40-850) via a variable optical attenuator (EXFO FVA-3150). The photoreceiver was either connected to an error analyzer (SHF 11100B) to measure the bit error rate (BER) or a 70 GHz equivalent time sampling oscilloscope (Agilent Infiniium DCA-J 86100C) to record eye diagrams. With a bias current of 3.5 mA and a modulation voltage of 0.4 V_{pp}, error-free transmission (defined as BER$<10^{-12}$) was possible up to 20 Gb/s. The BER versus received optical power at 10, 15, and 20 Gb/s and the corresponding eye diagrams are shown in Fig. 5. The corresponding extinction ratio is 5.5dB in all cases. The bias current is close to the thermal rollover current, which is needed for a sufficiently high bandwidth and sufficient damping. Even so, the resonant behavior causes overshoot in the optical signal, which translates into timing jitter in the limiting photoreceiver [12]. The junction temperature at this current, estimated from the dissipated power and the thermal impedance, is 98°C.

V. Conclusion

We have presented results from a study of the dynamic characteristics of 850-nm-wavelength hybrid-cavity VCSELs heterogeneously integrated on silicon using DVS-BCB adhesive bonding. A 5 μm oxide aperture VCSEL has a 3dB modulation bandwidth exceeding 11 GHz, mainly limited by thermal effects and parasitics. While the capacitance can be reduced by adding more oxide layers in future designs, the thermal effects impose a more severe limitation. This calls for proceeding investigations of e.g. the use of integrated metallic heat spreaders for improved thermal performance. Still, the hybrid-cavity VCSEL was shown to support 20 Gb/s data transmission.

References

[1] E. Haglund *et al.*, "30 GHz bandwidth 850 nm VCSEL with sub-100 fJ/bit energy dissipation at 25–50 Gbit/s," *Electron. Lett.*, vol. 51, no. 14, pp. 1096–1098, Jul. 2015.

[2] D. M. Kuchta *et al.*, "A 71-Gb/s NRZ modulated 850-nm VCSEL-based optical link," *IEEE Photon. Technol. Lett.*, vol. 27, no. 6, pp. 577–580, Mar. 15, 2015.

[3] P. Moser *et al.*, "56 fJ dissipated energy per bit of oxide-confined 850 nm VCSELs operating at 25 Gbit/s," *Electron. Lett.*, vol. 48, no. 20, pp. 1292–1294, Sep. 2012.

[4] Y. Wang *et al.*, "Vertical-cavity surface-emitting laser flip-chip bonding to silicon photonics chip," in *Proc. IEEE Opt. Interconnects Conf.*, vol. 6. Apr. 2015, pp. 122–123.

[5] Y. Tsunemi, N. Yokota, S. Majima, K. Ikeda, T. Katayama, and H. Kawaguchi, "1.55-μm VCSEL with polarization-independent HCG mirror on SOI," *Opt. Exp.*, vol. 21, no. 23, pp. 28685–28692, Nov. 2013.

[6] J. Ferrara, W. Yang, L. Zhu, P. Qiao, and C. J. Chang-Hasnain, "Heterogeneously integrated long-wavelength VCSEL using silicon high contrast grating on an SOI substrate," *Opt. Exp.*, vol. 23, no. 3, pp. 2512–2523, Feb. 2015.

[7] E. P. Haglund *et al.*, "Silicon-integrated short-wavelength hybrid-cavity VCSEL," *Opt. Exp.*, vol. 23, no. 26, pp. 33634–33640, Dec. 2015.

[8] D. A. Louderback, G. W. Pickrell, H. C. Lin, M. A. Fish, J. J. Hindi, and P. S. Guilfoyle, "VCSELs with monolithic coupling to internal horizontal waveguides using integrated diffraction gratings," *Electron. Lett.*, vol. 40, no. 17, pp. 1064–1065, Aug. 2004.

[9] G. C. Park *et al.*, "Hybrid vertical-cavity laser with lateral emission into a silicon waveguide," *Laser Photon. Rev.*, vol. 9, no. 3, pp. L11–L15, May 2015.

[10] S. Keyvaninia, M. Muneeb, S. Stanković, P. J. Van Veldhoven, D. Van Thourhout, and G. Roelkens, "Ultra-thin DVS-BCB adhesive bonding of III–V wafers, dies and multiple dies to a patterned silicon-on-insulator substrate," *Opt. Mater. Exp.*, vol. 3, no. 1, pp. 35–46, Jan. 2013.

[11] P. Westbergh, J. S. Gustavsson, B. Kögel, A. Haglund, and A. Larsson, "Impact of photon lifetime on high-speed VCSEL performance," *IEEE J. Sel. Topics Quantum Electron.*, vol. 17, no. 6, pp. 1603–1613, Nov. 2011.

[12] E. P. Haglund, P. Westbergh, J. S. Gustavsson, and A. Larsson, "Impact of damping on high-speed large signal VCSEL dynamics," *J. Lightw. Technol.*, vol. 33, no. 4, pp. 795–801, Feb. 15, 2015.

[13] P. P. Baveja *et al.*, "Impact of device parameters on thermal performance of high-speed oxide-confined 850-nm VCSELs," *IEEE J. Quantum Electron.*, vol. 48, no. 1, pp. 17–26, Jan. 2012.

[14] Y. Liu, W.-C. Ng, B. Klein, and K. Hess, "Effects of the spatial nonuniformity of optical transverse modes on the modulation response of vertical-cavity surface-emitting lasers," *IEEE J. Quantum Electron.*, vol. 39, no. 1, pp. 99–108, Jan. 2003.

[15] L. A. Coldren and S. W. Corzine, *Diode Lasers and Photonic Integrated Circuits*. Hoboken, NJ, USA: Wiley, 1995.

[16] N. Nishiyama, M. Arai, S. Shinada, K. Suzuki, F. Koyama, and K. Iga, "Multi-oxide layer structure for single-mode operation in vertical-cavity surface-emitting lasers," *IEEE Photon. Technol. Lett.*, vol. 12, no. 6, pp. 606–608, Jun. 2000.

[17] M. Azuchi, N. Jikutani, M. Arai, T. Kondo, and F. Koyama, "Multioxide layer vertical-cavity surface-emitting lasers with improved modulation bandwidth," in *Proc. 5th Pacific Rim Conf. Lasers Electro-Opt.*, vol. 1. 2003, p. 163.

[18] Y.-C. Chang, C. S. Wang, L. A. Johansson, and L. A. Coldren, "High-efficiency, high-speed VCSELs with deep oxidation layers," *Electron. Lett.*, vol. 42, no. 22, pp. 1281–1282, Oct. 2006.